Research Square

Preprints are preliminary reports that have not undergone peer review.
They should not be considered conclusive, used to inform clinical practice,
or referenced by the media as validated information.

Magnetically Assisted Assembly of Ni/Fe Catalysts for Efficient Oxygen Evolution Reaction

Rong Zhao

rong.zhao@udc.edu

University of the District of Columbia

Hayden Brown

University of the District of Columbia

Pawan Tyagi

University of the District of Columbia

Short Report

Keywords: Magnetically Assisted fabrication, Ni/Fe catalyst, Oxygen evolution reaction, Alkaline water splitting, Electrocatalysis

Posted Date: May 11th, 2026

DOI: https://doi.org/10.21203/rs.3.rs-9569411/v1

License: This work is licensed under a Creative Commons Attribution 4.0 International License.
Read Full License

Additional Declarations: No competing interests reported.

Abstract

A simple and rapid magnet-assisted fabrication strategy is developed to construct vertically aligned Ni/Fe wire architectures for the oxygen evolution reaction (OER). Ferromagnetic Fe powders are assembled into wirelike structures under an external magnetic field, followed by Ni electrodeposition to form a hierarchical catalyst. The resulting electrode exhibits a highly porous and aligned architecture with lengths on the millimeter scale, providing a large exposed surface area and open pathways for electrolyte penetration, gas release, and efficient mass transport. Electrochemical measurements show an overpotential of approximately 246 mV at 10 mA cm^{-2} and a Tafel slope of 60 mV dec^{-1}, indicating favorable catalytic activity and kinetics. The high double layer capacitance corresponds to a roughness factor of 77, indicating a substantially enlarged electrochemically active surface area (ECSA). The electrode also demonstrates excellent stability with negligible potential variation over 50 h of continuous operation, indicating good electrochemical stability. This work demonstrates a scalable and facile magnetically assisted fabrication strategy for constructing high-surface-area OER electrodes, offering a practical platform for tuning electrode morphology, catalyst loading, and Ni-Fe compositional and structural configuration in alkaline water splitting, and is extendable to other ferromagnetic material systems.

1 Introduction

The oxygen evolution reaction (OER) is a key half reaction in electrochemical water splitting, yet its sluggish multistep proton coupled electron transfer kinetics continue to limit the overall efficiency of hydrogen production systems [1, 2]. Developing active, stable, and cost effective OER electrocatalysts therefore remains a central challenge [3, 4]. Ni based materials have been widely studied in alkaline media due to their favorable activity, earth abundance, and scalability [5], while Fe incorporation has often been reported to further enhance performance in Ni based systems [6]. However, beyond composition, catalytic activity is strongly influenced by electrode architecture, accessible surface area, and charge and mass transport characteristics [7].

Ni based OER catalysts can be synthesized through a range of approaches that differ in complexity, structural control, and scalability. Simple methods such as electrodeposition and chemical precipitation enable direct and low-cost fabrication of Ni hydroxide or oxide materials, but often produce densely packed or randomly structured catalyst layers with limited active site exposure and restricted mass transport [8, 9]. In contrast, more advanced strategies, including hydrothermal synthesis [10–16], thermal treatment [17], templating approaches [18], and atomic layer deposition [19–22], provide improved control over nanostructure and surface area, but typically require multistep processing, longer reaction times, or specialized equipment. As a result, many high performance catalyst designs rely on increasingly complex fabrication routes, which can limit their practical scalability and direct integration into electrode systems. Therefore, there remains a need for fabrication strategies that can simultaneously achieve high surface area, enhanced active site accessibility, and scalable electrode construction without extensive synthetic complexity.

Here, for the first time, a magnetic field assisted structural assembly strategy is combined with electrodeposition to fabricate high performance Ni OER electrodes. Under an applied magnetic field, Fe wires are assembled into vertically aligned conductive scaffolds that are subsequently coated with Ni, enabling direct construction of three-dimensional electrodes with high electrochemically active surface area (ECSA) and efficient charge and mass transport pathways without multistep synthesis or high temperature processing. In this system, Fe primarily serves as a conductive and structurally directing scaffold for the subsequent Ni deposition. Compared with conventional electrodeposition, this method introduces controlled architectural organization that enhances surface accessibility, while maintaining simplicity, scalability, and direct electrode integration relative to more complex synthesis strategies. The resulting electrodes exhibit low overpotential at 10 mA cm^{-2}, favorable Tafel kinetics, a high electrochemical roughness factor, and stable long-term operation in alkaline conditions, demonstrating a practical route to engineer electrode architecture through magnetic field assisted assembly.

Importantly, this fabrication strategy offers intrinsic tunability, where magnetic field conditions influence scaffold alignment and morphology, while electrodeposition parameters such as current density and deposition time regulate catalyst loading and Ni:Fe configuration. Appropriate exposure of Fe can further modify the electronic structure of Ni to form NiFe like active sites, which further enhance catalytic performance [23, 24]. This approach provides a scalable platform for practical water splitting electrode design and alkaline electrolyzer applications and can be extended to other magnetic material systems for broader catalyst and electrode design.

2 Materials and Methods

2.1 Synthesis of Ni/Fe Catalysts

Iron (Fe) powder with a particle size of less than 44 μm (325 mesh) (Metal Powders USA, USA) was used to construct the scaffold. The powder was subjected to an external magnetic field generated by a permanent magnet, inducing the formation of vertically aligned wirelike structures oriented along the magnetic field on the stainless-steel substrate surface. Following scaffold assembly, Ni was electrodeposited onto the Fe scaffold using a VersaSTAT potentiostat (Princeton Applied Research, USA) in a commercial Goldeneye nickel electrolyte (Technic Inc., USA). Deposition was conducted in a three-electrode configuration, with the stainless-steel supported Fe scaffold as the working electrode, a Ni plate as the counter electrode, and an Ag/AgCl electrode as the reference. Regions outside the active catalyst area were masked with Kapton tape to prevent undesired Ni deposition. Potentiostatic deposition was performed at -1.2 V versus Ag/AgCl for 600 s at room temperature. At this applied cathodic potential, Ni^{2+} ions were reduced at the Fe scaffold surface, resulting in the formation of a Ni coated Fe electrode.

2.2 Characterization of Ni/Fe Catalysts

The surface morphology and microstructure of the Ni/Fe electrodes were characterized using a Phenom XL scanning electron microscopy (SEM) (Thermo Fisher Scientific, USA). Elemental composition was analyzed using energy dispersive X-ray spectroscopy (EDS) coupled with the SEM system to confirm the presence and relative abundance of Ni on the Fe scaffold.

2.3 Electrochemical Measurements

Electrochemical measurements were performed in a three-electrode configuration using 1 M KOH (ACS grade, Alliance Chemical, USA) as the electrolyte. The Ni/Fe electrode on stainless-steel was used as the working electrode, a stainless-steel mesh served as the counter electrode, and a Hg/HgO electrode was employed as the reference. Cyclic voltammetry (CV) was conducted within a non-faradaic potential window of 0.30 V to 0.40 V at scan rates of 10, 20, 40, 60, 80, and 100 mV s^{-1} to evaluate capacitive behavior. Additional CV scans were performed over a wider potential range of 0.0 V to 0.65 V at a scan rate of 1 mV s^{-1} to identify redox features associated with Ni species. Linear sweep voltammetry (LSV) was carried out from 0.0 V to 0.65 V at a scan rate of 1 mV s^{-1} to assess electrocatalytic activity. Electrochemical impedance spectroscopy (EIS) measurements were conducted at a fixed potential corresponding to approximately 10 mA cm^{-2} obtained from the LSV curve, using an AC amplitude of 5 mV over a frequency range from 100 kHz to 0.01 Hz.

3 Results and Discussion

3.1 Structural and Compositional Characterization

The fabricated Ni/Fe catalyst (Fig. 1a) exhibits a vertically oriented, wire like architecture with lengths on the order of several millimeters. The wires are uniformly distributed, indicating effective magnetic alignment during synthesis and good structural integrity. This configuration provides a large exposed surface area and open pathways for electrolyte penetration and bubble release, thereby enhancing catalytic activity and mass transport. SEM images (Fig. 1b) show that the wires have diameters on the order of tens of micrometers and form an interconnected structure. Their surfaces show granular and nodular features, resulting in hierarchical roughness that increases the accessible surface area. EDS analysis (Fig. 1c) confirms the successful deposition of Ni onto the Fe scaffold, with Ni as the dominant element (88.12 at%) and minor contributions from Fe (2.99 at%) and O (8.89 at%), where oxygen likely originates from surface oxidation. Overall, the results demonstrate that the magnet guided fabrication approach produces a high surface area Ni on Fe architecture with favorable characteristics for OER.

3.2 Electrochemical Performance

A representative CV scan of the Ni/Fe electrode (Fig. 2a) highlights the characteristic redox behavior associated with the Ni^{2+}/Ni^{3+} transition. A distinct anodic peak is observed during the forward scan at approximately 1.4 V vs. RHE, corresponding to the oxidation of Ni^{2+} to Ni^{3+} species. On the reverse scan, a cathodic peak appears at a lower potential around 1.33 V vs. RHE, which is attributed to the reduction

of Ni^{3+} back to Ni^{2+}. The clear presence of this redox couple indicates the formation of electrochemically active nickel oxyhydroxide species on the electrode surface. At higher potentials beyond the oxidation peak, the current density increases sharply, reflecting the onset of the OER. This behavior confirms the catalytic activity of the Ni/Fe electrode under alkaline conditions. The LSV polarization curve (Fig. 2b) was corrected with 90% iR compensation during post processing using the solution resistance (R□) obtained from EIS. The overpotential at 10 mA cm^{-2} is $\eta_{10} \approx 246$ mV vs. RHE. This performance is linked to the hierarchical structure of the magnet-guided architecture, which provides a high density of active sites and facilitates charge and mass transport. The presence of Fe may also contribute to the catalytic performance, although its specific role requires further investigation. The corresponding Tafel plot (Fig. 2c), derived from the iR corrected LSV data, exhibits a linear relationship between overpotential and the logarithm of current density, yielding a slope of approximately 60 mV dec^{-1}. This low value indicates favorable reaction kinetics and efficient charge transfer at the electrode electrolyte interface. EIS Nyquist plot (Fig. 2d) further supports this behavior, showing a well-defined semicircle characteristic of charge transfer controlled kinetics. Fitting with an equivalent circuit of R□ - (R_{ct} || CPE) yields R□ and R_{ct} values of approximately 0.96 Ω and 1.05 Ω, respectively, indicating low interfacial resistance. The double layer capacitance (C_{dl}) of the Ni/Fe catalyst was estimated from CV in the non-faradaic region at various scan rates, where the capacitive current density was obtained as half of the absolute difference between the anodic and cathodic current densities at a fixed potential of 0.35 V vs. Hg/HgO within the non-faradaic region. The capacitive current density exhibits a linear dependence on the scan rate, indicating a dominant double layer charging process. The slope of the linear fit yields a C_{dl} value of approximately 3.08 mF cm^{-2} (Fig. 2e). Assuming a specific capacitance of 0.04 mF cm^{-2}, the roughness factor was calculated to be approximately 77, indicating a substantially enlarged ECSA. This increased surface area provides a high density of accessible active sites and contributes to enhanced catalytic performance. Finally, the long-term stability of the Ni/Fe electrode (Fig. 2f) was evaluated at 10 mA cm^{-2} over a duration of 50 h. The potential exhibits minimal variation, increasing slightly from 1.478 V to 1.485 V, indicating excellent electrochemical stability. This minor change suggests that the electrode preserves its structural integrity while maintaining stable adhesion of the active layer under prolonged electrochemical operation, confirming the durability of the magnet guided wire architecture for sustained OER.

4 Conclusions

A magnet-assisted fabrication strategy is developed to construct vertically aligned Ni/Fe wire electrodes for the OER in alkaline media. Ferromagnetic Fe particles are assembled into ordered wirelike structures under an external magnetic field, followed by Ni electrodeposition to form a hierarchical catalyst without complex processing. The resulting porous and aligned architecture enhances electrolyte access, gas release, and charge transport while increasing ECSA. Electrochemical measurements indicate favorable activity, efficient kinetics, and stable long-term operation. This work demonstrates a simple and scalable

approach for engineering electrode architecture and catalyst integration, providing a practical platform for tuning morphology and Ni to Fe configuration in alkaline water splitting systems.

Declarations

Acknowledgements

This research was funded by the National Science Foundation CREST Award, grant number HRD-1914751.

Author Contributions

Rong Zhao: data collection and analysis, writing and editing; Hayden Brown: data collection and analysis; Pawan Tyagi: data analysis and editing, and funding.

Funding National Science Foundation CREST Award, grant number HRD-1914751.

Data Availability All data is available upon request.

Declarations Conflict of Interest The authors declare no competing interests.

Ethics and Consent to Participate NA.

Consent for Publication NA.

References

1. Ding H, Liu H, Chu W, Wu C, Xie Y (2021) Structural Transformation of Heterogeneous Materials for Electrocatalytic Oxygen Evolution Reaction. Chem Rev 121:13174–13212. https://doi.org/10.1021/acs.chemrev.1c00234
2. Liu Y, Zhou D, Deng T, He G, Chen A, Sun X, Yang Y, Miao P (2021) Research Progress of Oxygen Evolution Reaction Catalysts for Electrochemical Water Splitting. ChemSusChem 14:5359–5383. https://doi.org/10.1002/cssc.202101898
3. Zhang K, Zou R (2021) Advanced Transition Metal-Based OER Electrocatalysts: Current Status, Opportunities, and Challenges. Small 17:2100129. https://doi.org/10.1002/smll.202100129
4. Xie X, Du L, Yan L, Park S, Qiu Y, Sokolowski J, Wang W, Shao Y (2022) Oxygen Evolution Reaction in Alkaline Environment: Material Challenges and Solutions. Adv Funct Mater 32:2110036. https://doi.org/10.1002/adfm.202110036
5. Chen C, Olu P-Y, Fan R, Shen M (2025) Review of Ni-Based Materials for Industrial Alkaline Hydrogen Production. ChemSusChem 18:e202401415. https://doi.org/10.1002/cssc.202401415
6. Zhang X, Fang X, Zhu K, Yuan W, Jiang T, Xue H, Tian J (2022) Fe-doping induced electronic structure reconstruction in Ni-based metal-organic framework for improved energy-saving hydrogen

production via urea degradation. J Power Sources 520:230882. https://doi.org/10.1016/j.jpowsour.2021.230882

7. Sun S, Li H, Xu ZJ (2018) Impact of Surface Area in Evaluation of Catalyst Activity. Joule 2:1024–1027. https://doi.org/10.1016/j.joule.2018.05.003
8. Napari M, Huq TN, Hoye RLZ, MacManus-Driscoll JL (2021) Nickel oxide thin films grown by chemical deposition techniques: Potential and challenges in next-generation rigid and flexible device applications. InfoMat 3:536–576. https://doi.org/10.1002/inf2.12146
9. Kamble C, Jadhav VV, Mane RS (2023) Chapter 11 - Electrodeposition of metal oxide nanostructures. In: Mane R, Jadhav V, Al-Enizi A (eds) Solution Methods for Metal Oxide Nanostructures. Elsevier, pp 197–220
10. Yang L-X, Zhu Y-J, Tong H, Liang Z-H, Li L, Zhang L (2007) Hydrothermal synthesis of nickel hydroxide nanostructures in mixed solvents of water and alcohol. J Solid State Chem 180:2095–2101. https://doi.org/10.1016/j.jssc.2007.05.009
11. Tang Y, Liu Y, Yu S, Zhao Y, Mu S, Gao F (2014) Hydrothermal synthesis of a flower-like nano-nickel hydroxide for high performance supercapacitors. Electrochimica Acta 123:158–166. https://doi.org/10.1016/j.electacta.2013.12.187
12. Dong L, Chu Y, Sun W (2008) Controllable Synthesis of Nickel Hydroxide and Porous Nickel Oxide Nanostructures with Different Morphologies. Chem – Eur J 14:5064–5072. https://doi.org/10.1002/chem.200701627
13. Min S, Zhao C, Chen G, Qian X (2014) One-pot hydrothermal synthesis of reduced graphene oxide/Ni(OH)2 films on nickel foam for high performance supercapacitors. Electrochimica Acta 115:155–164. https://doi.org/10.1016/j.electacta.2013.10.140
14. Zhu Z, Wei N, Liu H, He Z (2011) Microwave-assisted hydrothermal synthesis of Ni(OH)2 architectures and their in situ thermal convention to NiO. Adv Powder Technol 22:422–426. https://doi.org/10.1016/j.apt.2010.06.008
15. Salavati-Niasari M, Seyghalkar H, Amiri O, Davar F (2013) Simple Hydrothermal Synthesis of Nickel Hydroxide Flower-Like Nanostructures. J Clust Sci 24:365–376. https://doi.org/10.1007/s10876-013-0558-3
16. Yang T, Yang L, Xie Y, Dai C, Li Z, Zhang S, Wang K, Li F, Jiang L, Sun Y (2025) Synthesis of NiS/Ni3S4/Ni3S2/NF Heterostructure as High-Efficiency Electrocatalyst for Oxygen Evolution Reaction. Catal Lett 155:335. https://doi.org/10.1007/s10562-025-05166-7
17. Davidson A, Tempere JF, Che M, Roulet H, Dufour G (1996) Spectroscopic Studies of Nickel(II) and Nickel(III) Species Generated upon Thermal Treatments of Nickel/Ceria-Supported Materials. J Phys Chem 100:4919–4929. https://doi.org/10.1021/jp952268w
18. Ghanem MA, Al-Mayouf AM, Singh JP, Arunachalam P (2017) Concurrent Deposition and Exfoliation of Nickel Hydroxide Nanoflakes Using Liquid Crystal Template and Their Activity for Urea Electrooxidation in Alkaline Medium. Electrocatalysis 8:16–26. https://doi.org/10.1007/s12678-016-0336-8

19. Yang TS, Cho W, Kim M, An K-S, Chung T-M, Kim CG, Kim Y (2005) Atomic layer deposition of nickel oxide films using Ni(dmamp)2 and water. J Vac Sci Technol A 23:1238–1243. https://doi.org/10.1116/1.1875172
20. Hidrogo-Rico MA, Nedev N, Horley P, Mendívil MI, Castillo-Saenz J, Martínez-Guerra E, Juarez-Perez EJ, Aguirre-Tostado FS, Susarrey-Arce A, Martínez-Guerra E (2025) Tailoring Nickel Oxide Thin Films: Comparative Study of Oxidizing Agents in Thermal and Plasma-Enhanced Atomic Layer Deposition. ACS Omega 10:422–438. https://doi.org/10.1021/acsomega.4c06606
21. Haghverdi Khamene S, van Helvoirt C, Tsampas MN, Creatore M (2023) Electrochemical Activation of Atomic-Layer-Deposited Nickel Oxide for Water Oxidation. J Phys Chem C 127:22570–22582. https://doi.org/10.1021/acs.jpcc.3c05002
22. van Limpt RTM, Lao M, Verheijen MA, Tsampas MN, Creatore M (2025) Thickness-Dependent Oxygen Evolution Reaction Performance of Atomic Layer Deposition Cobalt Oxide/Nickel Oxide Heterostacks. J Phys Chem C 129:12859–12869. https://doi.org/10.1021/acs.jpcc.5c04002
23. Wang Y, Qiao M, Li Y, Wang S (2018) Tuning Surface Electronic Configuration of NiFe LDHs Nanosheets by Introducing Cation Vacancies (Fe or Ni) as Highly Efficient Electrocatalysts for Oxygen Evolution Reaction. Small 14:1800136. https://doi.org/10.1002/smll.201800136
24. Zhao J, Zhang J-J, Li Z-Y, Bu X-H (2020) Recent Progress on NiFe-Based Electrocatalysts for the Oxygen Evolution Reaction. Small 16:2003916. https://doi.org/10.1002/smll.202003916

Figures

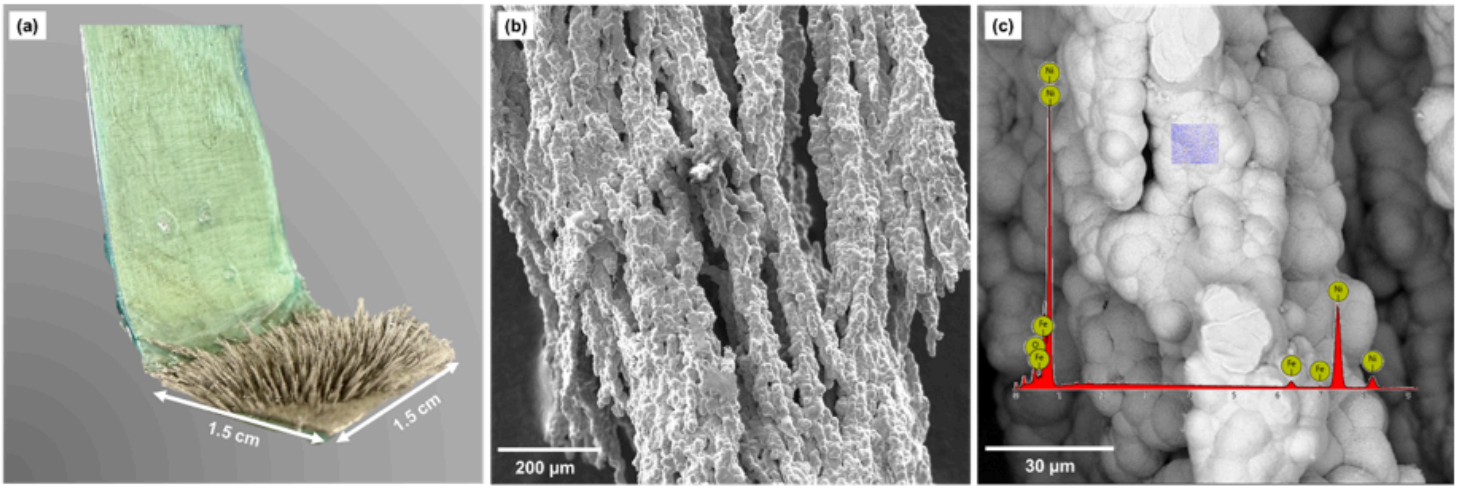


Figure 1

(a) Macroscopic photograph of the fabricated electrode, showing the dense Ni/Fe wire array formed on the stainless-steel substrate. (b) SEM image of the vertically aligned Ni/Fe wire architecture. (c) High magnification SEM image with corresponding EDS spectrum, confirming the presence of Ni, Fe, and O

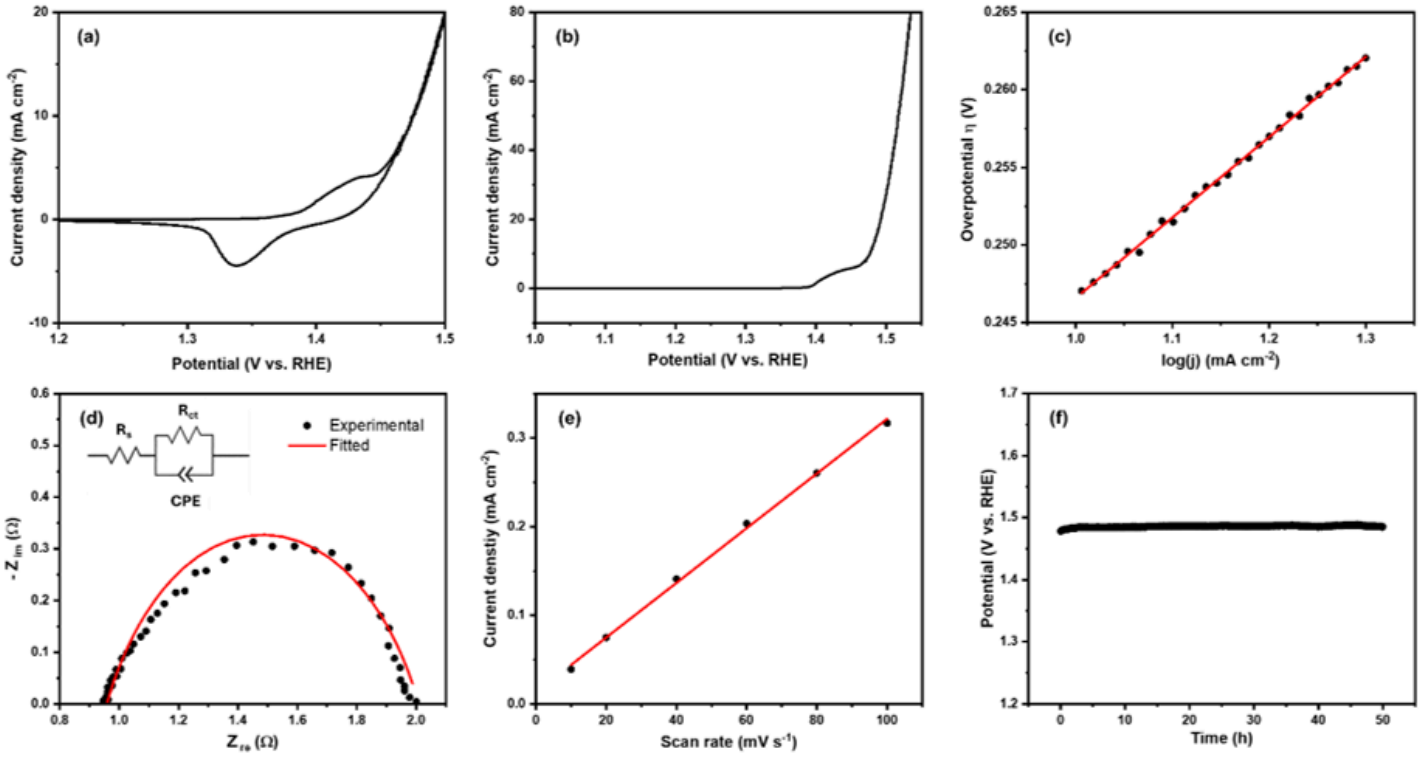


Figure 2

Electrochemical characterization of the Ni/Fe electrode in 1M KOH. (a) CV showing the Ni^{2+}/Ni^{3+} redox behavior. (b) iR corrected LSV polarization curve. (c) Tafel plot derived from LSV polarization data. (d) EIS Nyquist plot with equivalent circuit fitting. (e) Double layer capacitance estimation. (f) Chronopotentiometric stability test at 10 mA cm^{-2} over a duration of 50 h

Supplementary Files

This is a list of supplementary files associated with this preprint. Click to download.

- GraphicalAbstract.png